A Compressed Sensing Approach for MR Tissue Contrast Synthesis

Snehashis Roy, **Aaron Carass**, and **Jerry Prince**
Image Analysis and Communication Laboratory, Dept. of Electrical and Computer Engg., The Johns Hopkins University, USA, http://iacl.ece.jhu.edu/Prince

Snehashis Roy: snehashisr@jhu.edu; Aaron Carass: aaron_carass@jhu.edu; Jerry Prince: prince@jhu.edu

Abstract

The tissue contrast of a magnetic resonance (MR) neuroimaging data set has a major impact on image analysis tasks like registration and segmentation. It has been one of the core challenges of medical imaging to guarantee the consistency of these tasks regardless of the contrasts of the MR data. Inconsistencies in image analysis are attributable in part to variations in tissue contrast, which in turn arise from operator variations during image acquisition as well as software and hardware differences in the MR scanners. It is also a common problem that images with a desired tissue contrast are completely missing in a given data set for reasons of cost, acquisition time, forgetfulness, or patient comfort. Absence of this data can hamper the detailed, automatic analysis of some or all data sets in a scientific study. A method to synthesize missing MR tissue contrasts from available acquired images using an atlas containing the desired contrast and a patch-based compressed sensing strategy is described. An important application of this general approach is to synthesize a particular tissue contrast from multiple studies using a single atlas, thereby normalizing all data sets into a common intensity space. Experiments on real data, obtained using different scanners and pulse sequences, show improvement in segmentation consistency, which could be extremely valuable in the pooling of multi-site multi-scanner neuroimaging studies.

Keywords

compressed sensing; magnetic resonance imaging (MRI); image synthesis; phantom; standardization; segmentation; intensity normalization; histogram matching; histogram equalization

1 Introduction

Magnetic resonance (MR) imaging (MRI) is a noninvasive imaging modality that is the gold standard for imaging the brain. MR image processing, particularly segmentation of brain structures, has been used to further the understanding of normal aging or the progression of diseases such as multiple sclerosis, Alzheimer's disease, and schizophrenia. Large multi-site and multi-center studies are often used to gather more data across a broader population or to carry out follow-up imaging in longitudinal studies [12,16]. Because the intensities in conventional MR images do not have specific numerical units (unlike those in computed tomography (CT) images), there is a major concern about the consistency of quantitative results obtained in these studies due to the different pulse sequences [5] and scanners [11] that are used. In fact, because the intensity scale and the tissue contrast are dependent on the

MR acquisition pulse sequence as well as the underlying T_1, T_2, $T_2^{\star}$, P_D values in the tissue (cf. Fig. 1), any image processing task that is carried out on these data cannot normally be expected to behave quite the same across subjects. In this work, we focus on the consistency

of image processing tasks—particularly on the task of image segmentation—using conventionally acquired MR data.

Numerous methods have been proposed to find the segmentation of cortical and sub-cortical structures of the human brain. Some of these methods assume a statistical model [17] for the probability distribution function (pdf) of the image intensity and generate a segmentation rule based on a maximum likelihood (ML) estimation [8] or maximum a-priori (MAP) estimation of the pdf parameters. Another popular class of segmentation method is based on Fuzzy C-Means (FCM) [2] and its modifications [1]. But all of these methods are intrinsically dependent on the tissue contrast of the image, which is dependent on the acquisition parameters. Accordingly, the same data acquired under different pulse sequences or different scanners, having different contrasts, yielding inconsistent segmentations [5].

One way of reducing the segmentation inconsistency is intensity normalization. Some popular ways to do this are histogram equalization or histogram matching by non-rigid registration [15], intensity scaling based on landmarks [18], intensity correction by a global piecewise linear [19] or a polynomial mapping [14]. A common problem with these methods is that the histogram matching is never perfect with discrete valued images. Also landmark based methods are mostly initialized by manually chosen landmarks, which are time consuming to create and lack robustness. Another way to normalize involves the use of the peak intensities of white matter (WM) or gray matter (GM) [4] to match the image histogram to a target histogram by information theoretic methods [25]. Histograms of the segmented sub-cortical structures can also be matched to the individual histograms of the sub-cortical structures of a registered atlas [13]. It has been shown to produce consistent sub-cortical segmentation over datasets acquired under different scanners. In spite of their efficiency, all these methods are intrinsically dependent on the accuracy of the underlying segmentation of the image and the atlas-to-subject registration method. Another group of techniques have been proposed to include the MR acquisition physics into the segmentation methodology [21,11] to normalize all intensity images by their underlying T_1, T_2, $T_2^\star$ and P_D values. They suffer from the fact that many images are to be acquired with precise acquisition parameters, which is often not possible in large scale studies.

In this paper, we propose an <u>M</u>R <u>i</u>mage <u>e</u>xample-based <u>c</u>ontrast <u>s</u>ynthesis (MIMECS) method, that addresses the problem of intensity standardization over pulse sequences or scanners. We build upon the concepts of compressed sensing [3,9] to develop a patch matching approach, that uses patches from an atlas to synthesize different MR contrast images for a given subject. The primary purpose of MIMECS synthesis—and therefore the application for evaluation of its efficacy—is consistent segmentation across pulse sequences and scanners.

There are a few key differences with previous methods of intensity normalizations [19,18,25,4,13,11,21]. MIMECS is a pre-processing step to the segmentation. It neither needs to estimate T_1, T_2, P_D values, nor does it need the intrinsic MR acquisition parameters, like echo time (TE) or repetition time (TR). It also does not need landmarks or any atlas-to-subject registration, thus being fully automatic and independent of the choice of registration methods used in any subsequent processing. We use it to normalize a dataset which is acquired under different pulse sequences and on different scanners [12], thus having diverse contrasts. On this dataset, we show that MIMECS can normalize all the images to a particular contrast, that produce more consistent cortical segmentations compared to their original contrasts.

The paper is organized as follows. First, we briefly summarize compressed sensing in Sec 2.1. Then we describe the imaging model in Sec. 3.1 and the contrast synthesis algorithm is

explained in Sec. 3.3. A validation study with phantoms is described in Sec. 4.1. Then, we use MIMECS to simulate alternate pulse sequences and show its applicability as an intensity normalization and histogram matching process on a set of multi-site and multi-scanner data in Sec. 4.2.

2 Background

2.1 Compressed Sensing

We use the idea of compressed sensing in our MIMECS approach. Compressed sensing exactly recovers sparse vectors from their projections onto a set of random vectors [9,3] that need not form a basis. The idea behind compressed sensing comes from the fact that most of the signals that we observe are usually sparse, thus it is better not to observe the full signal, but a part of it, and reconstruct the whole signal from those small number of measurements.

Suppose we want to reconstruct a signal $\mathbf{x} \in \mathbb{R}^n$ which is s-sparse, i.e. has at most s non-zero elements. We want to observe another vector $\mathbf{y} \in \mathbb{R}^d$, $s < d < n$, such that each element of $\mathbf{y}$ can be obtained by an inner product of $\mathbf{x}$ and another vector from $\mathbb{R}^n$. Then, compressed sensing can be used to reconstruct $\mathbf{x} \in \mathbb{R}^n$ exactly from $\mathbf{y} \, \mathbb{R}^d$, with $\mathbf{y} = \mathbf{\Phi}\mathbf{x}$, $d < n$, $\mathbf{x}$ being s-sparse, $\mathbf{\Phi} \in \mathbb{R}^{d \times n}$. Thus, compressed sensing is also a way to reduce the dimension of the observed sparse data in a lossless way.

One approach for finding $\mathbf{x}$ is to solve

$$\widehat{\mathbf{x}} = \min \|\mathbf{x}\|_0 \text{ such that} \|\mathbf{y} - \mathbf{\Phi}\mathbf{x}\|_2^2 < \varepsilon_1, \tag{1}$$

where ε_1 is the noise in the measurement and $\| \cdot \|_0$ indicates the number of non-zero elements in the vector. Although this approach provides some simple conditions on $\mathbf{\Phi}$ [10], it is an NP-hard problem. Another approach is to solve

$$\widehat{\mathbf{x}} = \min \|\mathbf{x}\|_1 \text{ such that} \|\mathbf{y} - \mathbf{\Phi}\mathbf{x}\|_2^2 < \varepsilon_2, \tag{2}$$

where $\|\mathbf{x}\|_1$ is the L_1 norm of a vector. This is a convex problem and can be transformed into a linear program that can be solved in polynomial time. If ε_2 is unknown, Eqn. 2 can be written in the following form,

$$\widehat{\mathbf{x}} = \arg \min_{\mathbf{x}} \{ \|\mathbf{y} - \mathbf{\Phi}\mathbf{x}\|_2^2 + \lambda \|\mathbf{x}\|_1 \}, \tag{3}$$

where λ is a weighing factor. The sparsity on $\hat{\mathbf{x}}$ increases as λ increases.

It has been shown that if $\mathbf{\Phi}$ follows the global restricted isometry property (RIP) [3], then the solutions to Eqn. 1 and Eqn. 2 are identical and the optimal solution can be obtained by an L_1 minimization problem using Eqn. 3. This result is interesting because it has been shown that *random* subsets of incoherent matrices satisfy the RIP [24]. Thus, to reconstruct $\mathbf{x}$, it is possible to observe its projections onto a set of previously chosen incoherent vectors. We use this idea to find a sparse vector for each patch and then use that sparse vector as an index into the atlas.

3 Method

3.1 Imaging Model

Consider two MR images $\mathbf{Y}_1$ and $\mathbf{Y}_2$ of the same person, acquired at the same time, but having two different MR contrasts, C1 and C2, labeled as 1 and 2. E.g. $\mathbf{Y}_1$ and $\mathbf{Y}_2$ can be either T1-w, T2-w or PD-w images. They could be either 2D slices or 3D volumes. The imaging equations can be written as,

$$Y_1 = \mathscr{W}_1(T_1, T_2, P_D, T_2^\star, \Theta_1) + \eta_1 \tag{4}$$

$$Y_2 = \mathscr{W}_2(T_1, T_2, P_D, T_2^\star, \Theta_2) + \eta_2 \tag{5}$$

where Θ_1 and Θ_2 are the intrinsic imaging parameters, like TR, TE, flip angle etc for that particular acquisition, $\mathscr{W}_1$ and $\mathscr{W}_2$ are imaging equations [7] corresponding to the contrast or the pulse sequence used, η_1 and η_2 are random noise. T_1, T_2 and P_D are relaxation times and the proton density maps of the tissues. They could be 2D or 3D maps, according to $\mathbf{Y}_1$ and $\mathbf{Y}_2$.

Ideally, if a number of C1 contrast images of the subject is acquired, with the Θ's known for all the acquisitions, then an estimate of the underlying T_1, T_2 and P_D maps can be obtained by either directly inverting $\mathscr{W}_1$ in Eqn. 4 [11] or by a least square estimate [21]. Then $\mathbf{Y}_2$ can directly be synthesized using Θ_2 and the estimates of T_1, T_2 and P_D's using Eqn. 5.

There are several drawbacks for this strategy. Θ_1 and Θ_2 are often not known, $\mathscr{W}_1$ and $\mathscr{W}_2$ are difficult to model accurately or multiple acquisitions are not taken. Therefore, it is almost impossible to reconstruct $\mathbf{Y}_2$ from $\mathbf{Y}_1$ using the straight-forward approach. We will try to synthesize $\mathbf{Y}_2$ from $\mathbf{Y}_1$ using an atlas.

3.2 Atlas Description

Define an atlas $\mathcal{A}$ as a pair of images, $\mathcal{A} = \{\varphi_1, \varphi_2\}$, where φ_1 and φ_2 are C1 and C2 contrasts of the same subject having the same resolution. We assume that φ_1 and φ_2 are co-registered. Also assume that φ_1 and φ_2 are made of $p \times q \times r$ 3D patches. For convenience, we assume that each of the 3D patches is stacked into a 1D vector of size $d \times 1$, $d = p \times q \times r$. The patches are then denoted by $d \times 1$ vectors $\varphi_1(i)$ and $\varphi_2(i)$, $i \in \Omega_\varphi$. Ω_φ is the image domain of both φ_1 and φ_2, as they are co-registered. Then we define the C1 and C2 contrast dictionaries Φ_1 and $\Phi_2 \in \mathbb{R}^{d \times N}$, where the columns of Φ_1 and Φ_2 are patches $\varphi_1(i)$ and $\varphi_2(i)$, $i \in \Omega_\varphi$ from the atlas and $N = |\Omega_\varphi|$ is the number of patches from $\mathcal{A}$. Clearly, a column of Φ_1 corresponds to the same column in Φ_2.

3.3 Contrast Synthesis

Now, given a subject image $\mathbf{Y}_1$ of contrast C1, we want to generate its C2 contrast using Φ's. $\mathbf{Y}_1$ is first decomposed into $d \times 1$ patches $\mathbf{y}_1(j)$, $j \in \Omega_Y$, Ω_Y is the input image domain. The primary idea of MIMECS is that each subject patch $\mathbf{y}_1(j)$ can be matched to one or more patches from the dictionary Φ_1, because they are of the same C1 contrast. The matching patches have their own C2 contrast counterparts in Φ_2, which are then used to synthesize the C2 contrast version of $\mathbf{y}_1(j)$. As a result, the need of any atlas to subject registration is eliminated. This idea of patch matching can be explained efficiently using the idea of sparse priors [26] in a compressed sensing paradigm.

From Eqn. 4 and Eqn. 5, if $\mathcal{W}_1$ and $\mathcal{W}_2$ are linear operators of $\Theta = [T_1, T_2, T_2^\star, P_D, \Theta_1, \Theta_2]$, then a pseudo-inverse on Eqn. 4 will provide Y_2 from Y_1. Ignoring noise, the reconstruction of Y_2 can be written as,

$$Y_2 = GY_1, \quad G = \mathcal{W}_2(\mathcal{W}_1^T \mathcal{W}_1)^{-1} \mathcal{W}_1^T Y_1. \tag{6}$$

This inverse problem is ill-posed because G is almost always never known. The problem is regularized by assuming that any patch $y_1(j)$ can be found from a rich and over-complete dictionary Φ_1, having the same contrast as $y_1(j)$, by

$$y_1(j) \approx \Phi_1 x_1(j), \ \text{for some } x_1(j) \in \mathbb{R}^N, \ \text{with} \left\| x_1(j) \right\|_0 \ll N, \ j \in \Omega_Y. \tag{7}$$

$\| \cdot \|_0$ is the L_0 norm, denoting number of non-zero elements in a vector. Intuitively, the sparsest representation $x_1(j)$ denotes an index of Φ_1, such that $y_1(j)$ is matched to a particular column of Φ_1. This regularized problem is written in a compressed sensing paradigm following Eqn. 3,

$$x_1(j) = \arg\max_\alpha [\left\| y_1(j) - \Phi_1 \alpha \right\|_2^2 + \lambda \left\| \alpha \right\|_1], \ \alpha \geq 0, \ j \in \Omega_Y, \tag{8}$$

where λ is a weighing factor, as defined in Eqn. 3. A positivity constraint on the sparse representation $x_1(j)$ is enforced to impose a valid anatomical meaning on the elements of $x_1(j)$, such that an element of $x_1(j)$ denotes a positive weight of how much a column of Φ_1 contributes in reconstructing $y_1(j)$. This positivity constraint was previously explored in Lasso [23].

With the sparse representation of $y_1(j)$, we simply reconstruct the C2 contrast patch as,

$$\widehat{y}_2(j) = \Phi_2 x_1(j). \tag{9}$$

Then the C2 contrast image Y_2 is reconstructed by combining all the $\hat{y}_2(j)$'s thus obtained.

3.4 Contrast Synthesis with Modified Dictionary

Typically for a $256 \times 256 \times 198$ image volume, number of example patches $N \approx 100,0000$. It is computationally very intensive to work with Φ_1 that is of the order of $27 \times 100,0000$. To reduce the computation overhead, we use a dictionary selection procedure that uses an approximate segmentation of the input image. The rationale can be seen from the fact that if a patch $y_1(j)$ is known to come from a certain tissue type, e.g., pure white matter (WM), the computation of Eqn. 8 can be reduced by choosing a subset of Φ_1 that contains only pure WM patches.

We break down Φ_1, as well as Φ_2, into several sub-dictionaries of separate tissue classes, which are obtained from a topology preserving anatomy driven segmentation, called TOADS [1]. The atlas φ_1 is segmented into 6 tissue classes, namely cerebro-spinal fluid (CSF), ventricles, gray matter (GM), white matter (WM), basal ganglia and thalamus, labeled $l \in L = \{1, \ldots, 6\}$, respectively. The segmentation of φ_1, denoted as S_φ, is similarly decomposed into patches $s_\varphi(i)$, $i \in \Omega_\varphi$. The sub-dictionaries $\Phi_1^{(l)}$ and $\Phi_2^{(l)}$ for each tissue class l are generated as,

$$\forall i \in \Omega_\varphi, \ \varphi_1(i) \in \mathbf{\Phi}_1^{(l)}, \ \varphi_2(i) \in \mathbf{\Phi}_2^{(l)}, \ \text{if } l \text{ is an element of } \mathbf{s}_\varphi(i). \tag{10}$$

Fig. 2(a)–(c) show atlas SPGR and MPRAGE contrasts (φ_1 and φ_2) and their segmentation ($\mathbf{S}_\varphi$).

In our experiments, typically, $|\mathbf{\Phi}_1^{(l)}| \approx 10,000$ for a $256 \times 256 \times 198$ image. With the smaller atlas sub-dictionaries, we modify Eqn. 8 so as to reduce the search space for $\mathbf{y}_1(j)$'s. An approximate segmentation of $\mathbf{Y}_1$, denoted as $\mathbf{S}_Y$, is computed using one iteration of TOADS (e.g., Fig.2(d)–(e)). $\mathbf{S}_Y$ is again decomposed into patches $\mathbf{s}_Y(j)$, $j \in \Omega_Y$, so that the information about the tissue classes for $\mathbf{y}_1(j)$ is obtained from $\mathbf{s}_Y(j)$. Now, the contrast synthesis algorithm described in Eqn. 8–9 is modified with the inclusion of the sub-dictionaries,

1. Divide the atlases φ_1, φ_2 and the segmentation $\mathbf{S}_\varphi$ into $d \times 1$ patches, and generate the sub-dictionaries $\mathbf{\Phi}_1^{(l)}$ and $\mathbf{\Phi}_2^{(l)}$ according to Eqn. 10.

2. Find an approximate segmentation of the input C1 contrast $\mathbf{Y}_1$ as $\mathbf{S}_Y$. Divide the $\mathbf{Y}_1$ and $\mathbf{S}_Y$ into $d \times 1$ patches $\mathbf{y}_1(j)$'s and $\mathbf{s}_Y(j)$'s, $j \in \Omega_Y$.

3. For each j, find all the tissue classes l that $\mathbf{s}_Y(j)$ contains, $l \in L$.

4. For each j, generate patch specific dictionaries $\mathbf{\Phi}_1(j)$ by concatenating all $\mathbf{\Phi}_1^{(l)}$'s and $\mathbf{\Phi}_2(j)$ by concatenating $\mathbf{\Phi}_2^{(l)}$'s, $l \in L$. Thus $\mathbf{\Phi}_1(j)$ contains all the potential classes that $\mathbf{y}_1(j)$ could belong to, according to its atlas based approximate segmentation. Clearly, $\mathbf{\Phi}_1(j), \mathbf{\Phi}_2(j) \in \mathbb{R}^{d \times N_j}$ with $N_j \ll N$. At this point, if $\mathbf{\Phi}_1(j)$ becomes too large, we randomly choose a $d \times N_0$ random subset of $\mathbf{\Phi}_1(j)$ and the corresponding subset of $\mathbf{\Phi}_2(j)$ for further analysis to minimize computational overhead, $N_0 < N_j$.

5. Solve Eqn. 8 with $\mathbf{y}_1(j)$ and $\mathbf{\Phi}_1(j)$ to get $\mathbf{x}_1(j)$.

6. Solve Eqn. 9 with $\mathbf{\Phi}_2(j)$ and $\mathbf{x}_1(j)$ thus obtained.

7. Repeat for every $j \in \Omega_Y$.

4 Results

4.1 Estimation of λ

We use $3 \times 3 \times 3$ patches in all our experiments. All the images are normalized so that their peak WM intensities are unity. The optimal value of λ is obtained using a cross-validation study on the Brainweb phantoms [6] following the idea of homotopy methods [20]. We use the atlas C1 contrast as a T1-w (φ_1) and C2 as a T2-w (φ_2) phantom having 0% noise, shown in Fig. 3(a)–(b). Now, using these two phantoms as atlas, we use the same φ_1 phantom as the test image $\mathbf{Y}_1$ and try to reconstruct its T2-w contrast $\hat{\mathbf{Y}}_2$, while the true T2-w contrast is already known as $\varphi_2 = \mathbf{Y}_2$. The optimal λ is obtained by,

$$\widehat{\lambda} = \arg \min_{\lambda} \left\| Y_2 - \widehat{Y}_2 \right\|_2^2, \ \widehat{Y}_2 = \mathbf{\Phi}_2 \mathbf{X}(\lambda)$$
$$\text{such that } \mathbf{X}(\lambda) = \arg \min_{\alpha} [\left\| Y_1 - \mathbf{\Phi}_1 \alpha \right\|_2^2 + \lambda \left\| \alpha \right\|_1], \tag{11}$$

while $\mathbf{\Phi}_1$ and $\mathbf{\Phi}_2$ are obtained from φ_1 and φ_2 as defined earlier. λ is varied from [0.1, 0.8] and the optimal $\lambda = 0.5$ from Fig. 3(d). Using this λ, we generate a T2 contrast of the phantom shown in Fig. 3(c). Ideally, if we are to use all the patches from $\mathbf{\Phi}_1$ instead of

creating sub-dictionary $\boldsymbol{\Phi}_1^{(l)}$, $\hat{\lambda} \approx 0$. However, the use of a reduced sized dictionary gives improvement in computational efficiency with a sub-optimal performance, as seen from the reconstructed image (Fig. 3(c)). We use this lambda for all the subsequent experiments.

4.2 Experiment on BIRN Data

There has been concerns over consistency of the segmentations arising from scanner variability. To show that synthetic contrasts can produce consistent segmentations, we use the "traveling subject" data [12] that consists of scans of the same person under different pulse sequences and different scanners. These data were downloaded from the BIRN data repository, project accession number 2007-BDR-6UHZ1. We use the scans of 3 subjects, each consisting of one SPGR acquisitions from 1.5T GE, 4T GE, 1.5T Philips and 3T Siemens scanners each and one MPRAGE acquisition from a 1.5T Siemens scanner, each of them having $0.86 \times 0.86 \times 1.2$ mm resolution. One of the subjects is shown in Fig. 4(a)–(e). Their histograms are quite different (cf. Fig. 4(f)–(j)), and the Kullback-Leibler distance (KL distance) between each pair of the normalized histograms (Table 1) affirms this fact. This difference in histograms affect the consistency in the segmentations, shown in Fig. 4(k)–(o).

With the aim of having consistent segmentation of these images, we want to normalize the intensities of all the images to a particular target contrast. The purpose of choosing MPRAGE as the target C2 contrast is to have better delineation of cortical structures, because the GM-WM contrast is very poor on SPGR acquisitions. We use a GE 3T T1-w SPGR and its MPRAGE acquisitions from the BLSA study [16] as atlas φ_1 and φ_2, shown in Fig. 2(a)–(b). The synthesized images are shown in Fig. 5(a)–(e). It is seen from the images that they have more similar contrasts than the original images, and this is visually confirmed by the histograms in Fig. 5(f)–(j). Also, Table 1 shows that the the histograms of the synthetic MPRAGEs are more similar, having the KL distances being an order of magnitude less.

To show the improvement in segmentation consistency, we compare our method with a registration based approach, where we deformably register the SPGR atlas φ_1 to the SPGR input image $\mathbf{Y}_1$ by ABA [22] and use that transformation on φ_2 to generate the $\hat{\mathbf{Y}}_2$. Then the segmentation is performed on the registered images. If $\mathbf{Y}_1$ is MPRAGE (e.g. in Siemens 1.5T scanner), φ_2 is simply registered to $\mathbf{Y}_1$ to get $\hat{\mathbf{Y}}_2$. The Dice coefficients for the original, registered and transformed images and the synthetic images are shown in Table 2. Original images usually show poor consistency, especially between SPGR and MPRAGE acquisitions, which was already reported in literature [5]. Table 2 also shows that the Dice between SPGR and MPRAGE sequences is improved between the synthetic MPRAGE versions of the images compared to their original scans.

5 Conclusion

We have developed a compressed sensing based method, called MIMECS, that uses multiple contrast atlases to generate multiple contrasts of MR images. It is a patch-based method, where a patch in the subject C1 contrast image is matched to an atlas to generate a corresponding C2 contrast patch. An application of MIMECS is to normalize intensities between MR images taken from different scanners and different pulse sequences to generate synthetic images, while the synthetic images produce more consistent segmentation. In all our experiments, we have used only one pair of images as atlas to generate patch dictionaries. Also we have not particularly taken into account the topology of the structures. Our future work includes inclusion of features like topology and labels as a matching criteria, instead of only using intensities. Also we would like to explore the possibility of including more atlases and more contrasts.

Acknowledgments

References

1. Bazin PL, Pham DL. Topology-preserving tissue classification of magnetic resonance brain images. IEEE Trans on Medical Imaging. 2007; 26(4):487–496.

2. Bezdek JC. A Convergence Theorem for the Fuzzy ISO-DATA Clustering Algorithms. IEEE Trans on Pattern Anal Machine Intell. 1980; 20(1):1–8.

3. Candes EJ, Romberg JK, Tao T. Stable signal recovery from incomplete and inaccurate measurements. Comm on Pure and Appl Math. 2006; 59(8):1207–1223.

4. Christensen JD. Normalization of brain magnetic resonance images using histogram even-order derivative analysis. Mag Res Imaging. 2003; 21(7):817–820.

5. Clark KA, Woods RP, Rottenber DA, Toga AW, Mazziotta JC. Impact of acquisition protocols and processing streams on tissue segmentation of T1 weighted MR images. NeuroImage. 2006; 29(1): 185–202. [PubMed: 16139526]

6. Cocosco CA, Kollokian V, Kwan RKS, Evans AC. BrainWeb: Online Interface to a 3D MRI Simulated Brain Database. NeuroImage. 1997; 5(4):S425. http://www.bic.mni.mcgill.ca/brainweb/.

7. Deichmann R, Good CD, Josephs O, Ashburner J, Turner R. Optimization of 3-D MP-RAGE Sequences for Structural Brain Imaging. NeuroImage. 2000; 12(3):112–127. [PubMed: 10875908]

8. Dempster AP, Laird NM, Rubin DB. Maximum Likelihood from Incomplete Data via the EM Algorithm. Journal of Royal Stat Soc. 1977; 39:1–38.

9. Donoho DL. Compressed sensing. IEEE Trans Inf Theory. 2006; 52(4):1289–1306.

10. Elad M, Bruckstein AM. A Generalized Uncertainty Principle and Sparse Representation in Pairs of Bases. IEEE Trans Inf Theory. 2002; 48(9):2558–2567.

11. Fischl B, Salat DH, van der Kouwe AJW, Makris N, Segonne F, Quinn BT, Dale AM. Sequence-independent segmentation of magnetic resonance images. NeuroImage. 2004; 23(1):69–84.

12. Friedman L, Stern H, Brown GG, Mathalon DH, Turner J, Glover GH, Gollub RL, Lauriello J, Lim KO, Cannon T, Greve DN, Bockholt HJ, Belger A, Mueller B, Doty MJ, He J, Wells W, Smyth P, Pieper S, Kim S, Kubicki M, Vangel M, Potkin SG. Test-Retest and Between-Site Reliability in a Multicenter fMRI Study. Human Brain Mapping. 2008; 29(8):958–972. [PubMed: 17636563]

13. Han X, Fischl B. Atlas Renormalization for Improved Brain MR Image Segmentation Across Scanner Platforms. IEEE Trans Med Imag. 2007; 26(4):479–486.

14. He R, Datta S, Tao G, Narayana PA. Information measures-based intensity standardization of MRI. Intl Conf Engg in Med and Biology Soc. Aug.2008 :2233–2236.

15. Jager, F.; Nyul, L.; Frericks, B.; Wacker, F.; Hornegger, J. Bildverarbeitung für die Medizin 2008 Informatik aktuell. Vol. ch 20. Springer; Heidelberg: 2007. Whole Body MRI Intensity Standardization.

16. Kawas C, Gary S, Brookmeyer R, Fozard J, Zonderman A. Age-specific incidence rates of Alzheimer's disease: the Baltimore Longitudinal Study of Aging. Neurology. 2000; 54(11):2072–2077. [PubMed: 10851365]

17. Leemput KV, Maes F, Vandermeulen D, Suetens P. Automated Model-Based Tnumber Classification of MR Images of the Brain. IEEE Trans on Med Imag. 1999; 18(10):897–908.

18. Madabhushi A, Udupa JK. New methods of MR image intensity standardization via generalized scale. Med Phys. 2006; 33(9):3426–3434. [PubMed: 17022239]

19. Nyul LG, Udupa JK. On Standardizing the MR Image Intensity Scale. Mag Res in Medicine. 1999; 42(6):1072–1081.

20. Osborne MR, Presnell B, Turlach BA. A new approach to variable selection in least squares problems. IMA J Numerical Analysis. 2000; 20(3):389–403.

21. Prince JL, Tan Q, Pham DL. Optimization of MR Pulse Sequences for Bayesian Image Segmentation. Medical Physics. 1995; 22(10):1651–1656. [PubMed: 8551990]

22. Rohde GK, Aldroubi A, Dawant BM. The adaptive bases algorithm for intensity-based nonrigid image registration. IEEE Trans on Med Imag. 2003; 22:1470–1479.

23. Tibshirani R. Regression Shrinkage and Selection via the Lasso. J Royal Stat Soc. 1996; 58(1): 267–288.

24. Tropp JA, Gilbert AC. Signal recovery from random measurements via orthogonal matching pursuit. IEEE Trans Inform Theory. 2007; 53:4655–4666.

25. Weisenfeld NI, Warfield SK. Normalization of Joint Image-Intensity Statistics in MRI Using the Kullback-Leibler Divergence. Intl Symp on Biomed Imag (ISBI). Apr.2004 1:101–104.

26. Yang J, Wright J, Huang T, Ma Y. Image Super-Resolution Via Sparse Representation. IEEE Trans Image Proc. 2010; 19(11):2861–2873.
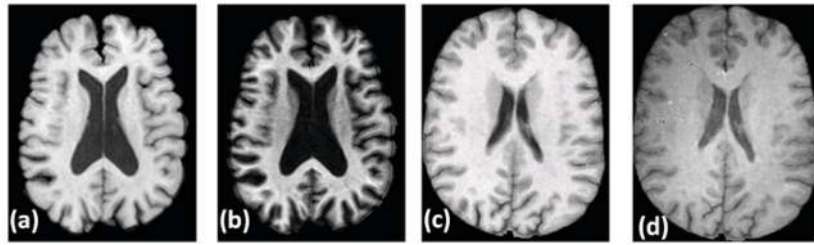
Fig. 1.
Data acquired under different pulse sequences or different scanners: **(a)** An acquisition of a Spoiled Gradient Recalled (SPGR) sequence in GE 3T scanner [16], **(b)** same subject with Magnetization Prepared Rapid Gradient Echo (MPRAGE) sequence in GE 3T scanner, **(c)** another subject [12], SPGR, GE 1.5T scanner, **(d)** same subject with MPRAGE sequence in a Siemens 3.0T scanner. Evidently, tissue contrast is dependent on the choice of pulse sequences, as well as on the choice of scanner. The contrast is intrinsically dependent on the choice of MR acquisition parameters, like flip angle, repetition time, echo time *etc.*
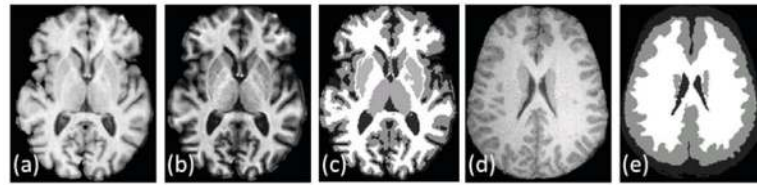
Fig. 2.
Modified dictionary using segmentation: **(a)** An example SPGR T1-w contrast atlas image φ_1 [16] from a GE 3T scanner, **(b)** its MPRAGE T1-w contrast φ_2, **(c)** their TOADS [1] segmentation $\mathbf{S}_\varphi$, used to generate the sub-dictionaries $\mathbf{\Phi}_1^{(l)}$ and $\mathbf{\Phi}_2^{(l)}$ according to Eqn. 10, **(d)** An SPGR T1-w subject image $\mathbf{Y}_1$ [12], **(b)** an approximate hard segmentation $\mathbf{S}_Y$ (obtained from TOADS), used to choose a reduced sub-dictionary
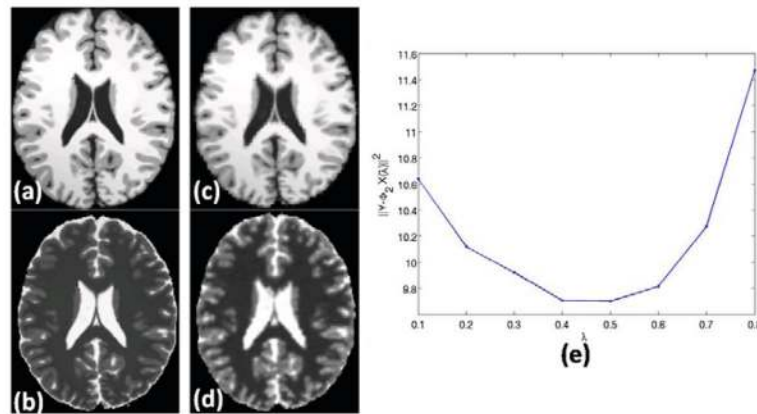
Fig. 3.
Optimal λ: **(a)** A T1-w Brainweb phantom φ_1 [6], **(b)** original T2-w version φ_2, they are used as atlas. **(c)** Reconstructed T1-w image $\Phi_1 \mathbf{X}(\hat{\lambda})$, from Eqn. 11, **(d)** Reconstructed T2-w image ($\hat{\mathbf{Y}}_2 = \Phi_2 \mathbf{X}(\hat{\lambda})$) using $\mathbf{Y}_1 = \varphi_1$, **(e)** plot of λ vs. the reconstruction error $\left\| Y_2 - \widehat{Y}_2 \right\|_2^2$.
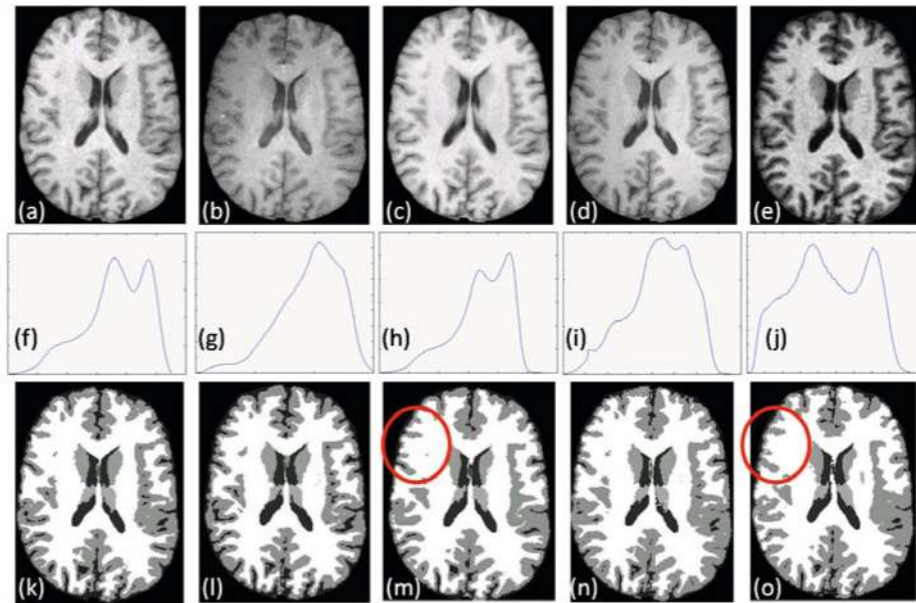
Fig. 4.
BIRN data: T1-w SPGR contrasts from **(a)** GE 1.5T, **(b)** GE 4T, **(c)** Philips 1.5T, **(d)** Siemens 3T scanner, **(e)** T1-w MPRAGE contrast from Siemens 1.5T. Their histograms are shown in **(f)**–**(j)** and the hard segmentations [1] are shown in **(k)**–**(o)**. The histograms are quite different which is reflected on the difference in the segmentations.
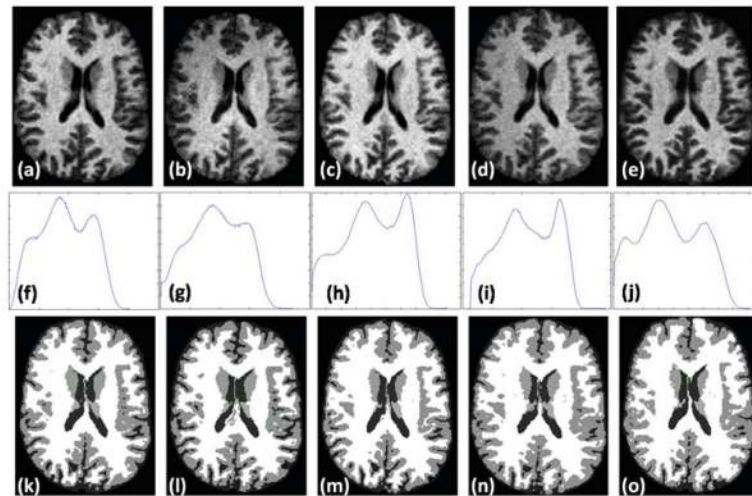
Fig. 5.
Synthesizing MPRAGE contrast from BIRN data: Synthetic MPRAGE contrasts of the data
shown in Fig. 4(a)–(e) using the atlas shown in Fig. 2(a)–(c). The histograms of the
synthetic MPRAGEs are shown in **(f)**–**(j)** and the hard segmentations [1] are shown in **(k)**–
(o).

Table 1

KL distances between original/synthesized image histograms for images acquired under 5 different scanners, averaged over 3 subjects

	GE 1.5T	GE 4T	Philips 1.5T	Siemens 3T	Siemens 1.5T
GE 1.5T	.	0.28/0.04	0.39/0.06	0.30/0.02	0.49/0.03
GE 4T	0.72/0.04	.	1.22/0.02	0.11/0.06	0.91/0.07
Philips 1.5T	0.48/0.05	0.85/0.23	.	0.88/0.04	0.07/0.07
Siemens 3T	0.53/0.01	0.07/0.04	0.98/0.03	.	0.88/0.06
Siemens 1.5T	0.62/0.03	1.01/0.06	0.05/0.01	1.04/0.08	.

Table 2

Consistency comparison: Segmentation consistency is measured on original 4 SPGR and 1 MPRAGE scans, their MPRAGE registered and transformed versions (described in Sec. 4.2) and synthesized MPRAGEs. Mean Dice coefficients, averaged over CSF, GM and WM, are reported between the segmentations of (original, registered, synthetic) images acquired under 5 different scanners/pulse sequences (GE 1.5T SPGR, GE 4T SPGR, Philips 1.5T SPGR, Siemens 3T SPGR and Siemens 1.5T MPRAGE) averaged over 3 subjects.

	GE 1.5T	GE 4T	Philips 1.5T	Siemens 3T	Siemens 1.5T
GE 1.5T	.	0.81, 0.78, 0.84	0.77, 0.83, 0.85	0.86, 0.87, 0.89	0.82, 0.80, 0.87
GE 4T	.	.	0.70, 0.71, 0.79	0.79, 0.77, 0.84	0.76, 0.77, 0.82
Philips 1.5T	.	.	.	0.78, 0.83, 0.84	0.74, 0.75, 0.84
Siemens 3T	.	.	.	.	0.78, 0.81, 0.85